

Mesoscale modeling of failure in partially sintered metals and homogenization to macroscale

Nathanaël Durr, Martin Sauer

Fraunhofer Institute for High-Speed Dynamics, Freiburg, Germany

Abstract:

In this paper, we present a methodology for the multiscale analysis of deformation and failure of partially sintered metals. This methodology is based on experimental investigations, mesoscale modeling with the finite element method (FEM), and transfer of relationships derived at the mesoscale to the macroscale using a homogenization process. It can be used to investigate structure-properties relationships and is illustrated for a specific type of copper.

The material is produced from cold-pressed spherical powder sintered at 700°C. Based on the statistical analysis of micrographs, three-dimensional voxel-based representative volume elements were generated. From these RVE's, finite element models were built. The material data for these mesoscopic models was derived partly from literature and partly from fitting simulated homogenized stress-strain response to experimental tensile tests. LS-Dyna's node-split feature was used to model failure within the RVE. Using homogenized stress-strain relationships obtained from RVE simulations with different loading types, a macroscale material model which includes non-linear plastic hardening and the dependence of failure strain on stress triaxiality was derived. This model is used in a macroscopic compression simulation and compared with a corresponding experimental result. Finally, an application of the mesoscopic model for fragmentation analysis illustrates possible future applications.

Keywords:

mesoscale, macroscale, RVE, failure, homogenization, sintered metal, quasi-static, impact

1 Introduction

The ability to predict the influence of manufacturing parameters on the behavior of polygranular materials under impact loads could speed up the material development process in areas such as defense technology, chemical processing, refining, etc. The behavior of such materials is governed by a number of factors. Apart from loading and sample geometry, the mechanical properties of grains and grain interfaces, i.e. the mesoscopic material properties, and the mesoscopic material structure, i.e. grain and pore sizes, shapes and orientations, play an important role. In this paper, for the example of partially sintered metals, we give an overview on the steps that are required for both mesoscale material modeling as applied for mesoscopic fragmentation analysis in [1], and the derivation of homogenized material laws. The latter can be used in a dynamic analysis on the macroscopic scale. A methodology similar to the one presented here was used in [2] for an open-cell aluminum foam.

The first and second steps are the construction of Representative Volume Elements (RVEs) at the mesoscale and the derivation of the required material laws. The third step is the construction of a continuum-mechanical model at the macroscale. For this purpose, different loading states are numerically investigated at the RVE scale using the commercial software LS-DYNA. The analysis of the homogenized results is made possible by using equivalent quantities. The homogenized plastic behavior, a pressure-density relationship and a triaxiality-dependent failure criterion can then be derived. As an example for one step towards model validation, the analysis of a cylinder compression test and the comparison to experimental results are given. Finally, mesoscopic impact computations show the potential of the mesoscopic model for fragmentation analysis.

2 Construction of the RVE

2.1 Definition of the RVE topology

Figure 1 shows micrographs obtained by chemical etching of three materials after cold-pressing at 300 MPa and subsequent sintering at 700°C. Manufacturing of the samples was done at the branch of the Fraunhofer Institute for Manufacturing Technology and Applied Materials Research (IFAM) in Dresden, Germany. From left to right, the materials are copper, iron and their mixture. Pores appear as black areas on the micrograph. For the mixture (third picture), the bright grains are copper and the dark ones are iron.

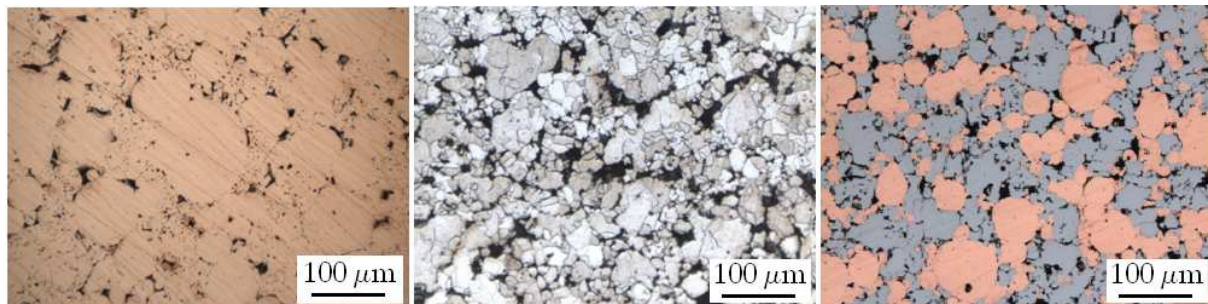


Figure 1: Micrographs of copper, iron and their mixture cold pressed at 300 MPa and sintered at 700°C.

The analysis of a set of micrographs allowed the progressive reconstruction of the 3D topology of a mesoscopic volume. Voxel-based RVEs were generated at the “Fraunhofer Institut für Techno- und Wirtschaftsmathematik” (ITWM) in Kaiserslautern, Germany, using their software GEODICT [3]. A graphical representation of an RVE is given in Figure 2, left.

To reduce the computational effort, smaller volumes were extracted from the original RVEs. Their representativeness was ensured by checking that the material response was conserved as the size of the volume decreased. The most optimal RVE was characterized by a 0.4 mm edge length and about 500 grains. In order to account for grain boundary failure, which is a typical phenomenon in partially

sintered metals, an artificial “border” material with a thickness of at least one voxel was inserted between metallic grains, see Figure 2, right.

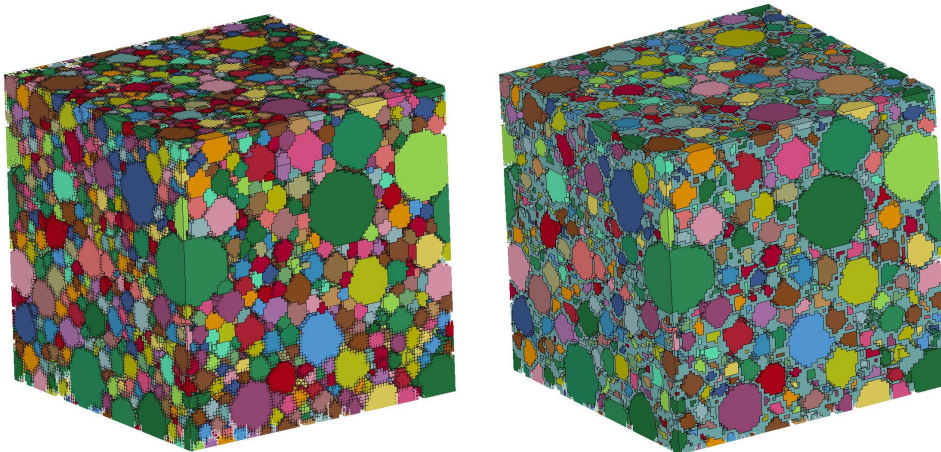


Figure 2: Left: computer-generated, voxel-based mesoscopic representative volume element (RVE) of copper pressed at 300 MPa and sintered at 700°C; right: same RVE after insertion of artificial “border” elements which represent the grain boundaries.

2.2 Mesoscale Material and Failure Modeling

In the following, the material of study will be copper cold-pressed at 300 MPa and sintered at 700°C.

2.2.1 Elastic-plastic parameters

Each of the two materials constituting the RVE, bulk copper and grain boundary material, is modeled with a piecewise linear elastic-plastic law, as shown in Figure 3. The material data for bulk copper was taken from the literature and consists of the following parameters: yield strength σ_Y , Young’s modulus E and plastic hardening modulus E_{tan} .

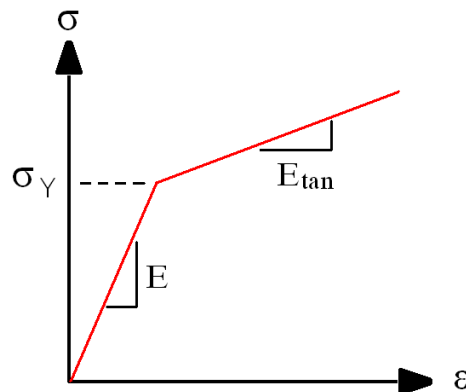


Figure 3: Schematic linear elastic – plastic material law used for copper grains. σ_Y denotes the yield strength, E is Young’s modulus, E_{tan} is the plastic hardening modulus.

Material parameters for the border material were determined by fitting computed homogenized mesoscopic material response to macroscopic experimental quasi-static tensile test results, as explained later in paragraph 2.2.3.

2.2.2 Failure law

As we deal with partially sintered metallic grains with relatively weak grain boundaries, we consider that only inter-granular failure can occur, without any intra-granular failure. A simple method to model failure in LS-DYNA would be to use plastic strain as an erosion criterion and thus delete elements that

reach a specified plastic strain level. However, this method has to be used carefully, see e.g. [4], and would lead to an undesired loss of volume in any case.

To avoid this issue, an alternative method was used, called node-split method (card TIED_NODES in LS-DYNA). It is based on a failure criterion at interface nodes. In order to use this method, nodes which are linked to different grains need to be duplicated for each grain. When the failure threshold (effective plastic strain) is reached in adjacent elements, the coincident nodes are permitted to separate from each other. Figure 4 shows an exemplary propagation of a crack between two grains.

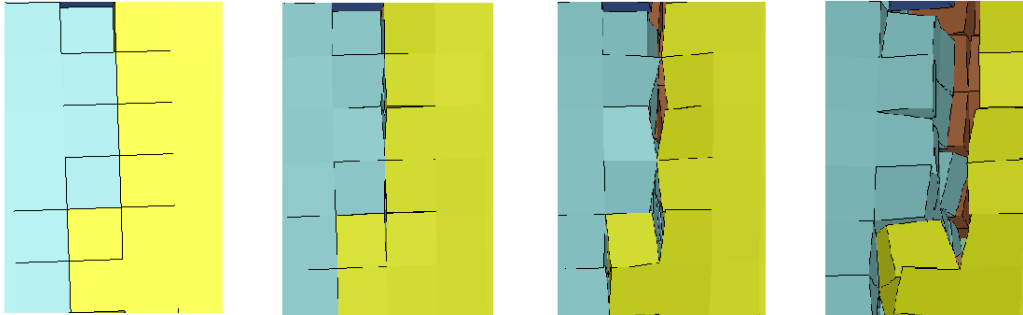


Figure 4: Crack propagation at a grain interface modeled with the node-split method.

Alternatively, the TIED_SURFACE_TO_SURFACE or TIEBREAK_SURFACE_TO_SURFACE options for contact could have been used, or cohesive elements in combination with one of the cohesive materials (MAT_COHESIVE). However, the strain-hardening like behavior at relatively low stress levels that was observed for this material (see below) could only be reproduced by assuming plastic hardening in a weaker “border” material, not by adjusting grain boundary failure parameters.

At RVE scale, the failure criterion leads to a progressive fragmentation pattern as shown for a tensile test, Figure 5.

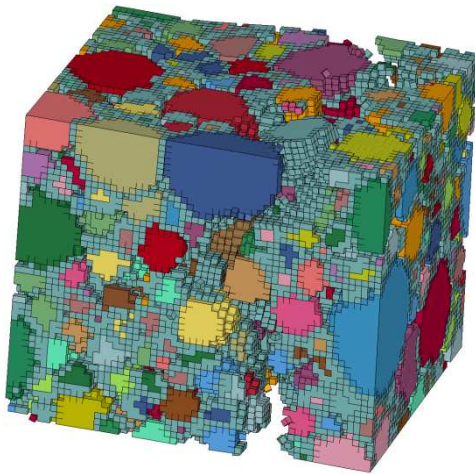


Figure 5: Fragmentation pattern of the RVE under uniaxial tensile test

2.2.3 Determination of unknown mesoscopic material parameters

As elasto-plastic parameters for the grains were taken from literature, the elastic-plastic parameters and the failure parameter of the border remained to be defined. For this purpose, the parameters were optimized by fitting homogenized stress-strain curves to experimental curves from quasi-static tensile tests. To make the comparison with the experiments possible, a homogenization of the mesoscopic variables needs to be performed. This consists in an averaging of all local variables in the RVE, as the following formulas show:

$$\bar{\varepsilon} = \frac{1}{V} \int_V \varepsilon \, d\tilde{V} \tag{1}$$

$$\bar{\sigma} = \frac{1}{V} \int_V \sigma \, d\tilde{V} \tag{2}$$

Eqn (1) and Eqn (2) correspond to the homogenization of the strain ε and the stress σ , respectively, averaged (or macroscopic) variables are topped by a dash.

Three separate aspects of the material response were optimized, see also Figure 6:

1. Optimization of the homogenized stress. This stress is determined by the initial yield stress of the border material.
2. Optimization of the plasticity curvature: a “statistic” failure model of the RVE at grain scale was realized by randomly varying the values of critical effective plastic strain at all inter-granular nodes within a selected failure interval. This allows the successive birth of cracks in the RVE during the loading and leads to a non-linear, softened stress increase (concave curvature).
3. Optimization of the global failure point: this point is also coupled to the damage of the RVE, a global stress decrease occurs when enough nodes have split after the neighboring elements reached the effective plastic strain criterion.

It should be stressed that the selected material model for the grain boundaries was that one with the smallest number of parameters which yields a good accordance of experimentally measured and homogenized simulated response. Of course, complexity could be added by using non-linear plastic hardening for the border material and non-uniform statistical distributions for the critical strain failure threshold.

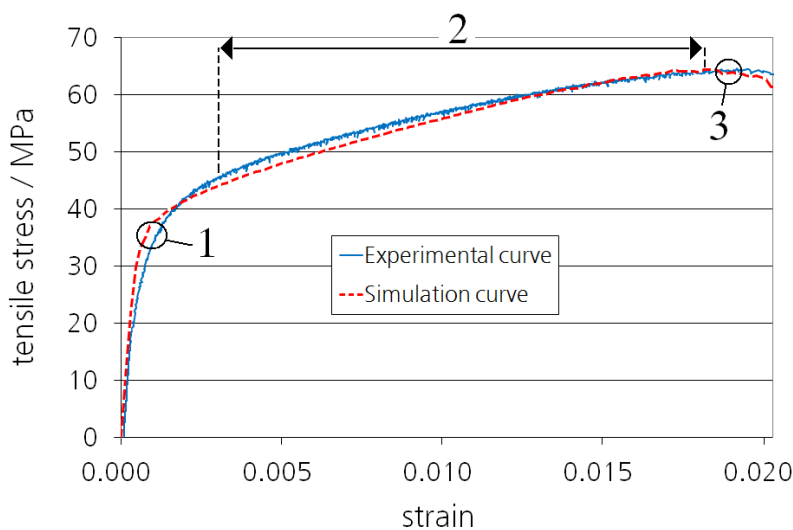


Figure 6: Fitting of the experimental and the simulated material responses.

Table 1 summarizes the parameters used for the studied material: Cu – 300 MPa – 700°C.

	Density (mg/mm ³)	Shear modulus (kPa)	Bulk modulus (kPa)	Hardening slope (kPa)	Yield stress (kPa)	Failure strain interval
Metallic grains	8.96	4.6 E7	1.29 E8	2.0 E4	7.0 E6	-
Border elements					4.0 E4	[0.029; 0.053]

Table 1: Summary of all parameters used for the RVE model: Cu – 300 MPa – 700°C.

3 Mesoscale Modeling Results, Homogenization and Simplified Macroscale Model

The heterogeneous mesoscopic model can be used to derive a homogeneous macroscopic model (homogenization). To achieve this, different loadings were applied to the RVE, these were uni- and multiaxial loadings, either with traction or compression.

Equivalent quantities for stresses and strains are commonly used to analyze different loading states. We used quantities based on the von Mises definition:

$$\bar{\sigma}_{\text{vM}} = \sqrt{\frac{3}{2}} (\bar{s}_{ij} : \bar{s}_{ij}) \quad (3)$$

$$\bar{\epsilon}_{\text{eff}}^{\text{pl}} = \sqrt{\frac{3}{2}} (\bar{\epsilon}_{ij}^{\text{pl}} : \bar{\epsilon}_{ij}^{\text{pl}}) \quad (4)$$

Eqn (3) and Eqn (4) define the von Mises stress $\bar{\sigma}_{\text{vM}}$ and the equivalent plastic strain $\bar{\epsilon}_{\text{eff}}^{\text{pl}}$, where \bar{s} is the deviatoric component of the stress tensor.

For each loading state, the equivalent stress was plotted over the equivalent strain, as shown in Figure 7. The simulated behavior can be approximated by a Johnson-Cook type exponential hardening, see Eqn (5). The parameters A, B and n are directly derived from the analysis of the flow curves:

$$\sigma_Y = \left(A + B \left(\epsilon_{\text{eff}}^{\text{pl dev}} \right)^n \right) \quad (5)$$

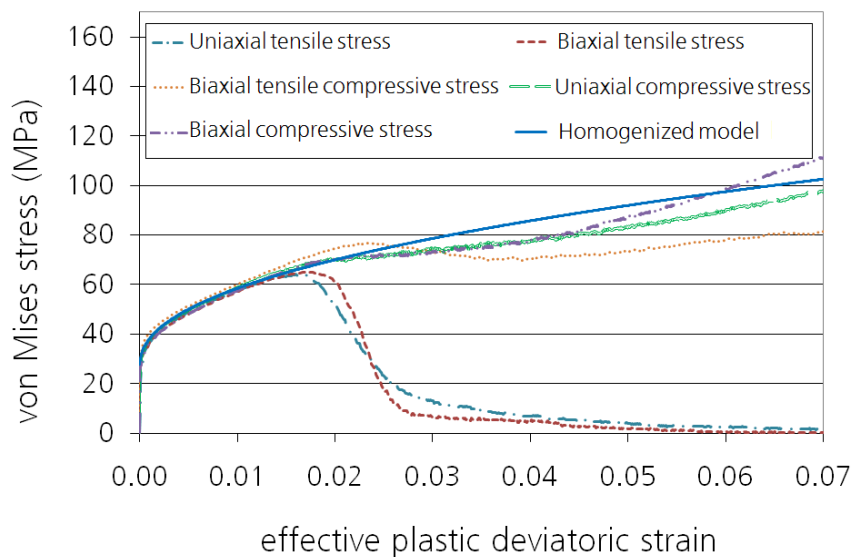


Figure 7: Homogenized stress evolution computed from the mesoscale model for different loading types, selected exponential hardening law for the homogenized model.

The analysis of the dependence of the effective plastic deviatoric strain at failure on the stress triaxiality σ^* , defined by Eqn (6), allows the definition of a simplified failure law. We used a simplified Johnson-Cook type failure law [5] as depicted in Eqn (7) and plotted on Figure 8. Here, p is the pressure, $\epsilon_{\text{eff}}^{\text{pl dev}}$ is the effective plastic deviatoric strain, and D_1 , D_2 and D_3 are model parameters.

$$\sigma^* = \frac{-p}{\sigma_{\text{vM}}} = \frac{\sigma_{11} + \sigma_{22} + \sigma_{33}}{\sigma_{\text{vM}}} \quad (6)$$

$$\epsilon_{\text{eff}}^{\text{pl dev}}(\text{failure}) = D_1 + D_2 \exp(D_3 \sigma^*) \quad (7)$$

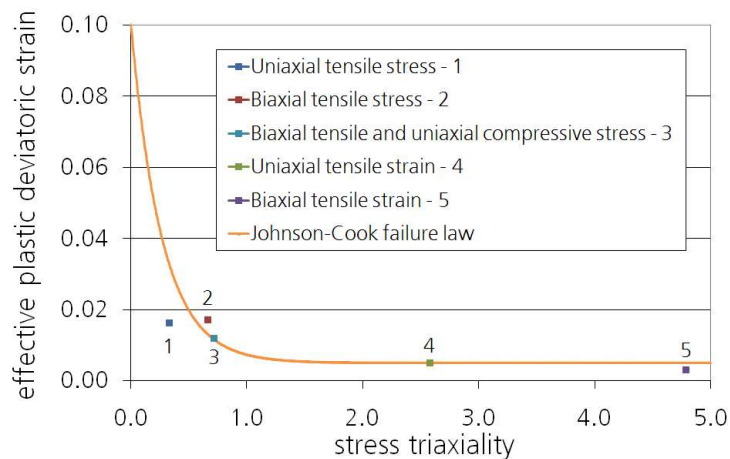


Figure 8: Triaxiality-dependent failure strain and Johnson-Cook failure law.

The homogenized failure law fits well to the homogenized mesoscale simulation results for triaxialities higher than 0.8. The strain increase in the homogenized behavior for small triaxialities ($\sigma^* < 0.8$) is motivated from the observation that no failure was observed in the mesoscale simulations of load cases with $\sigma^* \leq 0$ (Fig. 7, biaxial tensile-compressive, uniaxial and biaxial compressive stress cases).

A homogenized relation of pressure and volumetric strain was also derived from mesoscale simulations but will not be detailed here.

4 Validation of the homogenization: Compression Test

One first step in the validation of the homogenized model is outlined briefly in the following. In the experiment, a cylindrical sample is pressed between two plates. The experimental result is compared with the simulation of the same test in terms of the final sample size and the localization of cracks. Figure 9, left and middle, shows the simulation of the test before and after compression, respectively. A top view of the experimental and simulated samples at the end of the compression test is represented on Figure 9, right.

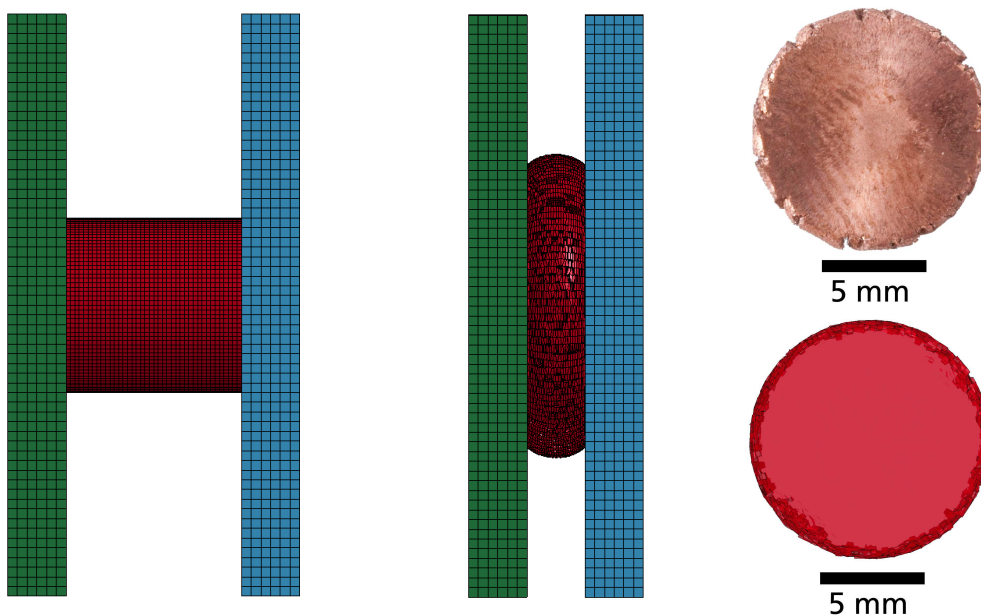


Figure 9: Left: cylinder placed between two rigid plates before compression test; middle: compressed cylinder and formation of cracks in an advanced stage of the compression test; right: top view of the compressed sample at the end of experiment and simulation.

The noticeable point on Figure 9, right, is the similarity of the formation of cracks on the periphery of the sample in both experimental and simulation cases.

The compressive stress was experimentally measured over the compressive strain and plotted together with the simulation result in Figure 10.

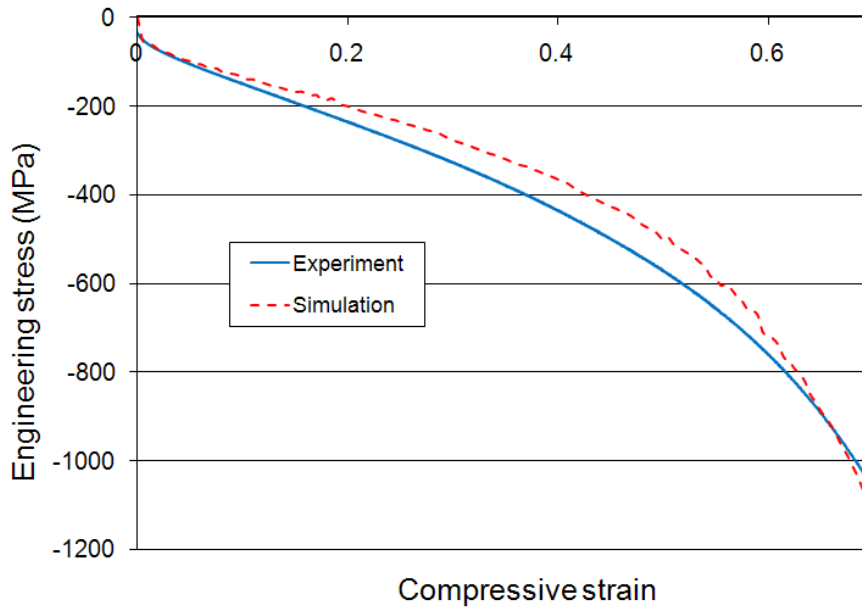


Figure 10: Numerical and experimental stress-strain curves by compression test.

Figure 10 shows a good accordance of the simulated and experimentally observed stress evolution over the strain, which shows that the macroscopic model developed by homogenization is applicable to this load case (quasi-static compression). Keeping in mind that the data base on which the mesoscopic model was built was kept as simple as possible and consisted only of the microstructural geometric features, linear elastic-plastic literature data for copper, and linear elastic-plastic and failure data for the border obtained by fitting to tensile tests, the accordance was actually better than expected.

5 Mesoscopic Fragmentation Simulation

The long-term objective of this work is to get a homogenized material model that would be able to reproduce, ideally, any loading state at any strain rate, including dynamic fragmentation under high- and hypervelocity impact. Currently, our model is limited to quasi-static cases.

Further dynamic simulations were performed at the mesoscale to evaluate possible mesoscopic inertia effects on the stress-strain response. In the calculations presented below, no strain rate dependency is incorporated in the mesoscopic material laws, instead, the values are identical to those identified through the process described in section 2.

A series of dynamic tensile loading simulations were with the RVE, strain rates ranged from 1 to 1000 s^{-1} . The results showed that below a strain rate of 100 s^{-1} , the stress-strain response was not sensitive to the strain rate. Only the tensile test at 1000 s^{-1} revealed a higher peak stress. From this observation, it was concluded that mesoscopic inertia effects induce velocity-dependent internal stress for high strain rates, but have no effect for lower strain rates in the present mesoscopic model. As in contrast, experiments showed a significant strain rate effect also at strain rates well below 1000 s^{-1} , some improvement in the mesoscopic model remains to be done to reproduce the observed strain rate dependency.

In spite of this deficit, further preliminary simulations involving impact fragmentation were performed at the mesoscale in order to investigate the usability of mesoscopic models for fragmentation prediction. The case considered was the perforation of a 0.8 mm-thick aluminum target plate by a cube with 3 mm side length. Two materials were investigated: the first cube was constituted of CuFe with a fabrication

pressure of 300 MPa and the second one of Fe with a fabrication pressure of 580 MPa. The mesoscopic models for these materials were derived in the same manner as for Cu 300 MPa, see section 2. Figure 11 and Figure 12 show a side view of the corresponding experiments done for two impact velocities: 1500 m/s and 2600 m/s.

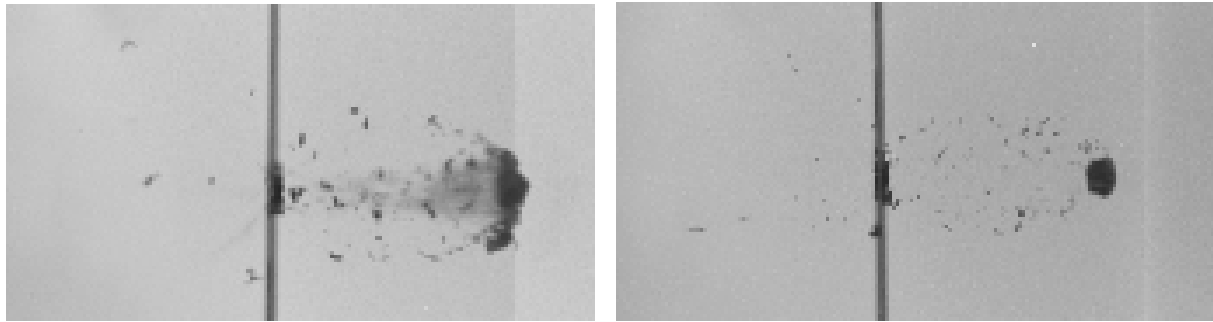


Figure 11: Perforation of an aluminum target plate (0.8 mm thickness) by a cube (3 mm side length); impact velocity: 1500 m/s; time after impact: 20 μ s. Left: CuFe 300 MPa; right: Fe 580 MPa. [1]

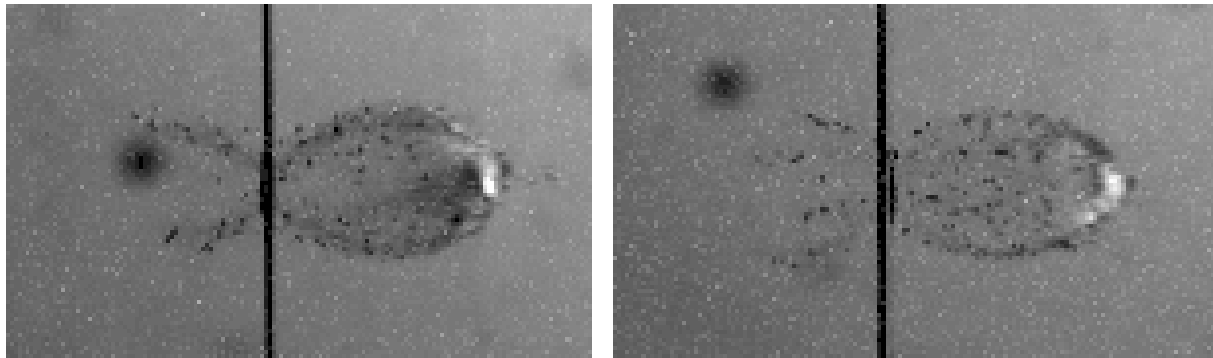


Figure 12: Perforation of an aluminum target plate (0.8 mm thickness) by a cube (3 mm side length); impact velocity: 2600 m/s; time after impact: 12 μ s. Left: CuFe 300 MPa; right: Fe 580 MPa. [1]

Figure 13 and Figure 14 show simulation results of cubes of size 0.4*0.4*0.4 mm on an aluminum plate of 0.1 mm thickness, which corresponds to “downscaled” versions of the above-presented tests. The “downscaling” is necessary for mesoscale simulations as the original cube size of 3 mm is so large that individual grains could not be represented in a computational mesh, the required number of elements would be far too big (the 0.4 mm edge length cube models already contain 125 000 solid elements). A comparably coarse mesh could be used for the plate in order to reduce computation times as we were primarily interested in the sintered material fragmentation. Although the results of the “downscaled” simulations are not directly comparable to the tests, they qualitatively reproduce some of the features that can be observed in the original tests. These features are:

1. Partly fragmentation occurs for low velocities (CuFe at 150 m/s, Fe at 475 m/s).
2. The weaker the material, the higher is the degree of fragmentation at a given velocity (compare Fe at 475 m/s yields approximately the same degree of fragmentation as CuFe at 150 m/s).
3. Complete fragmentation for Fe occurs at 1600 m/s and higher velocities.
4. The higher the velocity, the finer the fragments.
5. The hole in the aluminum plate generated by the perforation is rectangular for low and circular for high velocities.

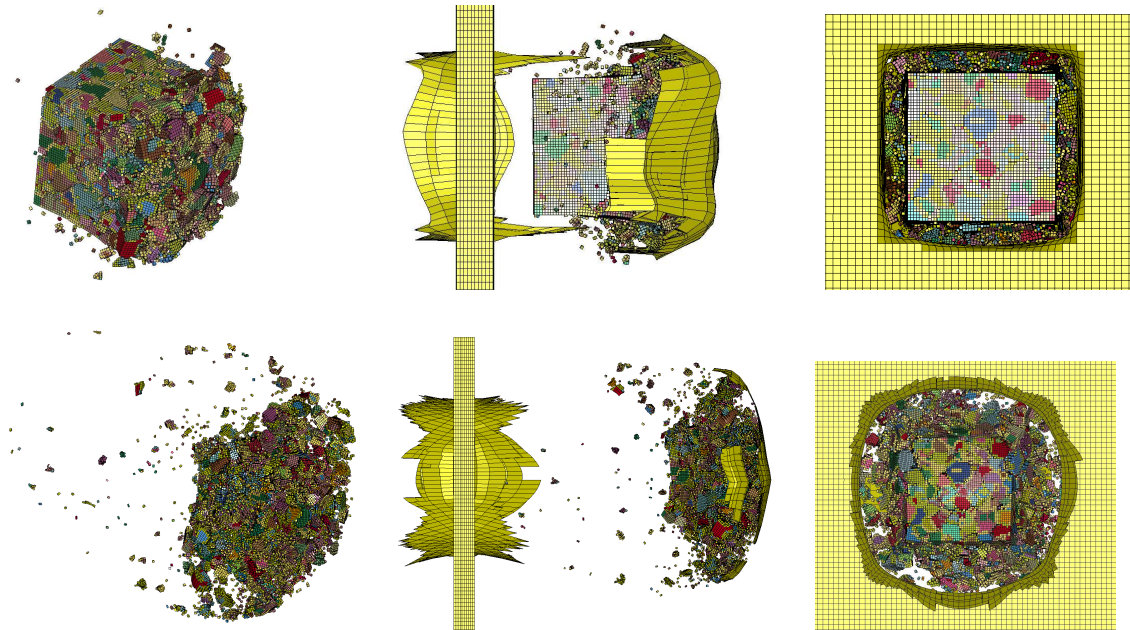


Figure 13: Mesoscale cube impact simulations for CuFe 300 MPa at 20 μ s after impact. Top: impact velocity 150 m/s, bottom: impact velocity 634 m/s. Left: slanted view of the cube after perforation, center: side view of plate and cube, right: view in shot direction.

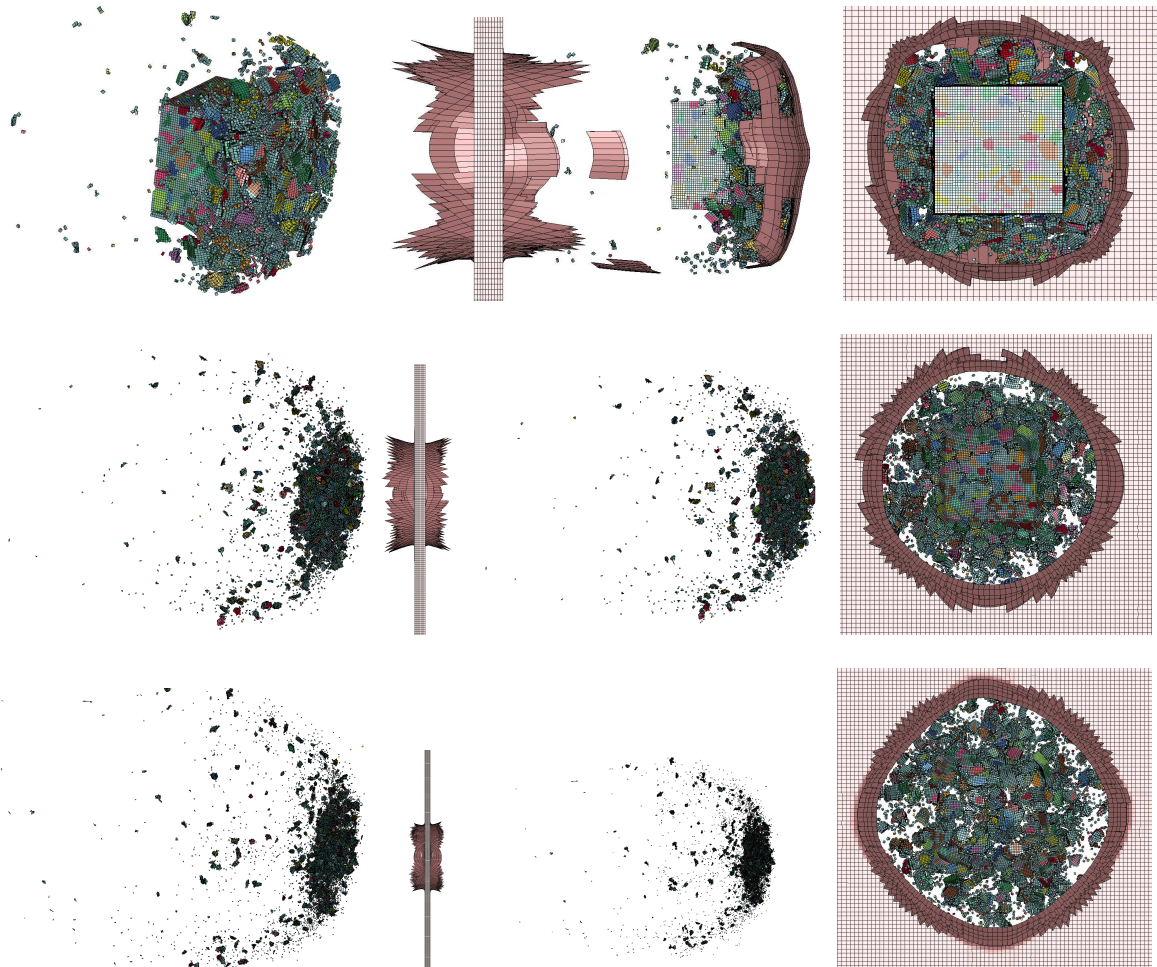


Figure 14: Mesoscale cube impact simulations for Fe 580 MPa at 20 μ s after impact. Top: impact velocity 475 m/s, middle: impact velocity 1600 m/s, bottom: impact velocity 2600 m/s. Left: slanted view of the cube after perforation, center: side view of plate and cube, right: view in shot direction.

6 Conclusion

The methodology for the multiscale analysis of deformation and failure of partially sintered metals outlined in this paper contains several steps. From microstructure analysis, a RVE that contains material and geometric information was built. Mesoscopic material parameters were determined by fitting homogenized simulation results to results of experimental tensile tests. The material model chosen was that one with the smallest number of parameters which yields a good accordance of experimentally measured and homogenized simulated response.

Further loading cases were simulated to characterize the material behavior at the mesoscale. The results were aggregated to allow the definition of homogeneous macroscopic material laws. As an example for validation of the macroscopic laws, a compressive test at macroscale confirmed the accordance of numerical and experimental results. The accordance was actually better than expected, keeping in mind that the data base on which the mesoscopic model was built consisted only of the microstructural geometric features and tensile tests.

The developed model remains open for further improvement, especially in the domain of the behavior under dynamic loading at higher strain rates. The possibility to conduct fragmentation analysis was illustrated by mesoscopic impact calculations.

7 Acknowledgements

We thank Frank Bagusat and Martin Lück from EMI who worked on the experimental results. The project was partly sponsored by the United States Department of the Navy, Office of Naval Research (ONR), under grant No. N00014-07-1-1053, this support is gratefully acknowledged.

8 References

- [1] Sauer, M.; Bagusat, F.; Durr, N; Klomfass, A.: Fragmentation of Partially Sintered Materials – Experimental Investigation and Mesoscale Simulation. Proceedings of the 11th Hypervelocity Impact Symposium, Freiburg 2010 (in print).
- [2] Wicklein, M.; Thoma, K.: Numerical investigations of the elastic and plastic behavior of an open-cell aluminum foam. Mat Sc. Eng., 2005, A 397: 391-399.
- [3] www.geodict.com
- [4] Schwer, L.: Aluminum plate perforation: a comparative case study using Lagrange with erosion, Multi-Material ALE, and Smoothed Particle hydrodynamics. Proc. 7th European LS-DYNA Conference, Salzburg, 2009: <http://www.dynalook.com/>.
- [5] Johnson, G.R.; Cook, W.H.: Fracture Characteristics of three metals subjected to various strains, strain rates, temperatures and pressures. Eng. Fract. Mech., 1985, 21: 31-48.

